



ΔΗΜΟΚΡΙΤΟΣ
ΕΘΝΙΚΟ ΚΕΝΤΡΟ ΕΡΕΥΝΑΣ ΦΥΣΙΚΩΝ ΕΠΙΣΤΗΜΩΝ



**Πανεπιστήμιο
Κρήτης**



**Πανεπιστήμιο
Πατρών**



“PROGRAM Thales – University of the Aegean – Determination of the Sources and the Physicochemical Properties of Fine and Ultrafine Particulate Matter (Aerosol) that affect the Climate of Greece”

ΠΡΑΞΗ «Θαλής - Πανεπιστήμιο Αιγαίου - Προσδιορισμός των Πηγών και των Φυσικοχημικών Ιδιοτήτων των Λεπτοκόκκων και Υπερλεπτοκόκκων Αιωρούμενων Σωματιδίων του Ατμοσφαιρικού Αερολύματος που επηρεάζουν το κλίμα της Ελλάδας»

**SECOND PROGRESS REPORT
ΔΕΥΤΕΡΗ ΕΝΔΙΑΜΕΣΗ ΕΚΘΕΣΗ**



INTRODUCTION

The purpose of the project is to identify and determine the sources and physicochemical processes through which the particulate matter (PM) produced / found in major cities of Greece and the Aegean region affect the climate. The aims of the project are:

1. The creation of a continuous network monitoring basic physicochemical properties using plethora of 'state of the art' instruments.
2. The identification of sources, concentrations and size of suspended particles in the larger cities of Greece (Athens, Thessaloniki and Patra) and the Aegean (Lesvos and Crete).
3. The assessment of the chemical composition of particulate matter, and how it changes during its stay in the atmosphere (AMS measurements and chemical analysis AS1).
4. The determination of the physicochemical properties of aerosols that affect the climate directly and indirectly (field measurements - Tandem DMA CCNC).
5. Perform measurements of the physicochemical properties of laboratory generated particles that simulate those observed in field measurements (laboratory measurements - Tandem DMA CCNC).
6. The development of parametric models (Theory Kohler, ISSOROPIA) and their comparison with the field measurements and laboratory experiments.
7. The identification and quantification of heterogeneous physicochemical processes between suspended particles, water vapor and air pollutants (NO_x, HNO₃, O₃) with the help of laboratory experiments and theoretical calculations.
8. The use of a new generation of 3D-CTMs for both the identification of area and the rate of production of new particles by nucleation, and to determine the number distribution and the chemical composition of aerosols.
9. Determination the physicochemical characteristics of aerosols that contribute most to the optical properties associated with the greenhouse effect.



10. Comparison of surface measurements with remote sensing measurements (MODIS).

The project includes seven actions, of which the first is the coordination of the project by the Professor of the Department of Environment Christodoulos Pilinis, while the last includes the external evaluation of the program. The other actions have purely scientific content. Since the Ministry has not informed us on the evaluation procedure, we, as a team, have decided to write the second progress report in English, in the case the evaluation process involves non-Greek speaking evaluators.

ΕΙΣΑΓΩΓΗ

Σκοπός του έργου είναι η διερεύνηση και ο προσδιορισμός των πηγών και των φυσικοχημικών διεργασιών μέσω των οποίων τα Αιωρούμενα Σωματίδια (ΑΣ) που παράγονται/συναντώνται σε μεγάλες πόλεις της Ελλάδας και στην περιοχή του Αιγαίου επηρεάζουν το κλίμα. Οι επιδιωκόμενοι στόχοι του έργου είναι:

1. Η δημιουργία σταθερού δικτύου παρακολούθησης βασικών φυσικοχημικών ιδιοτήτων με χρήση πληθώρας 'state of the art' οργάνων.
2. Ο προσδιορισμός των πηγών, συγκεντρώσεων και μεγέθους των αιωρούμενων σωματιδίων στις μεγαλύτερες πόλεις της Ελλάδας (Αθήνα, Θεσσαλονίκη και Πάτρα) και στην περιοχή του Αιγαίου (Λέσβο και Κρήτη).
3. Η εκτίμηση της χημικής σύστασης των αιωρούμενων σωματιδίων, και πώς αυτή μεταβάλλεται κατά την παραμονή τους στην ατμόσφαιρα (μετρήσεις AMS και χημική ανάλυση ΑΣ1).
4. Ο προσδιορισμός των φυσικοχημικών ιδιοτήτων των αιωρούμενων σωματιδίων που επηρεάζουν το κλίμα με άμεσο και έμμεσο τρόπο (μετρήσεις πεδίου Tandem DMA και CCNC).



5. Η διεξαγωγή μετρήσεων των φυσικοχημικών ιδιοτήτων εργαστηριακά παραγόμενων σωματιδίων που θα προσομοιώνουν αυτά που παρατηρούνται στις μετρήσεις πεδίου (εργαστηριακές μετρήσεις Tandem DMA και CCNC).
6. Η ανάπτυξη παραμετρικών μοντέλων (Θεωρία Kohler, ISSOROPIA) και σύγκριση με μετρήσεις πεδίου και εργαστηριακά πειράματα.
7. Ο ποιοτικός και ποσοτικός προσδιορισμός των ετερογενών φυσικοχημικών διεργασιών μεταξύ αιωρούμενων σωματιδίων, υδρατμών και ατμοσφαιρικών ρύπων (NO_x, HNO₃, O₃) με την διεξαγωγή εργαστηριακών πειραμάτων και θεωρητικών υπολογισμών.
8. Η χρήση νέας γενιάς 3D-CTM τόσο για τον προσδιορισμό των περιοχών και την ένταση παραγωγής νέων σωματιδίων με πυρηνοποίηση (nucleation), όσο και για τον προσδιορισμό του αριθμού της κατανομής και της χημικής σύστασης των αερολυμάτων.
9. Η εύρεση των φυσικοχημικών χαρακτηριστικών των αερολυμάτων που συνεισφέρουν περισσότερο στις οπτικές ιδιότητες που έχουν σχέση με το φαινόμενο του θερμοκηπίου.
10. Η σύγκριση των επίγειων μετρήσεων με τηλεπισκοπικές μετρήσεις (MODIS).

Το έργο περιλαμβάνει επτά δράσεις, εκ των οποίων η πρώτη αφορά τον συντονισμό από τον Καθηγητή του Τμήματος Περιβάλλοντος Χ. Πηλίνη και η τελευταία την εξωτερική αξιολόγηση του προγράμματος. Οι υπόλοιπες δράσεις είναι καθαρά επιστημονικού περιεχομένου.



PROGRESS SINCE THE FIRST PROGRESS REPORT

The progress of this research project per activity is described below:

Activity D1

During this coordination activity the following important actions took place since the first progress report:

- Using legal procedures all the chemicals needed for the next measurement campaigns were purchased.
- Organized the last of the three formal meetings in Heraklion (October 2014)
- Organized an extra experimental campaign.

Activity D2

This activity has been completed and described extensively in the first progress report.

Activities D3-D5

Sources and Chemical Characterization of Organic Aerosol during the Summer in the Eastern Mediterranean

During summer 2012 the concentration and chemical composition of fine particulate matter was measured in two Greek cities, Patras and Athens, in an effort to better understand the chemical processing of particles in the high photochemical activity environment of the Eastern Mediterranean. In both sites the composition of PM₁ was surprisingly similar to each other demonstrating the importance of regional sources for the corresponding pollution levels. The PM₁ average mass concentration was 9-16 µg



m^{-3} (Fig. 1). The contribution of sulphate was around 38%, while organic aerosol (OA) contributed approximately 45% in both cases. Nitrate was insignificant ($\sim 1\%$). The organic to carbon (O:C) mass ratio was 0.64 ± 0.10 in Patras and 0.58 ± 0.11 in Athens. In both cases the aerosol was acid (acidity: 0.75 ± 0.07 in Patras and 0.70 ± 0.09 in Athens).

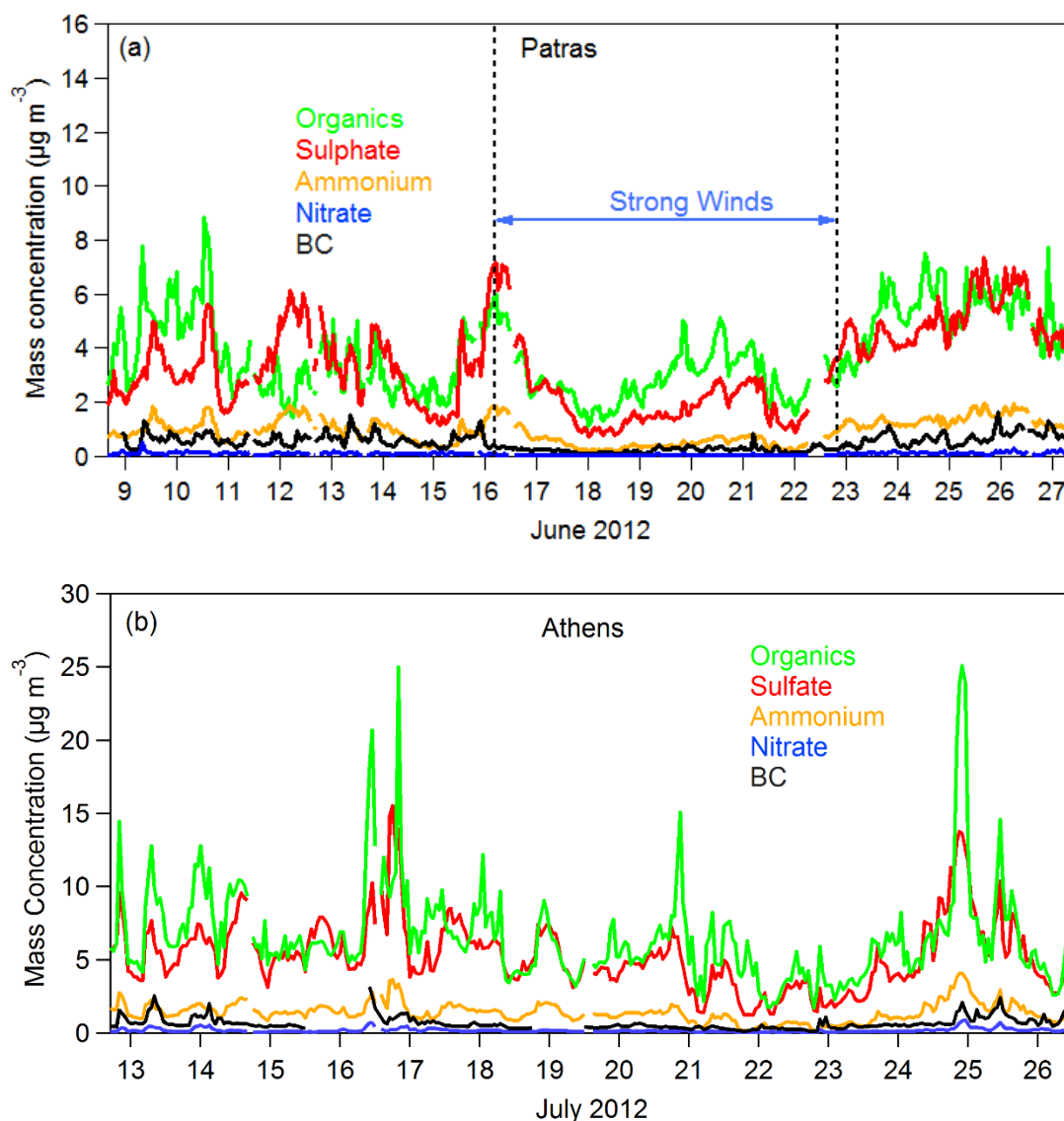


Figure 1. Time series of NR-PM₁ mass concentration measured by the AMS (corrected for the CE) a) for Patras and b) for Athens. The BC was provided by MAAP for Patras measurements and by an aethalometer for Athens campaign.

During the measurements in Patras not a single nucleation event was observed (Fig. 2).



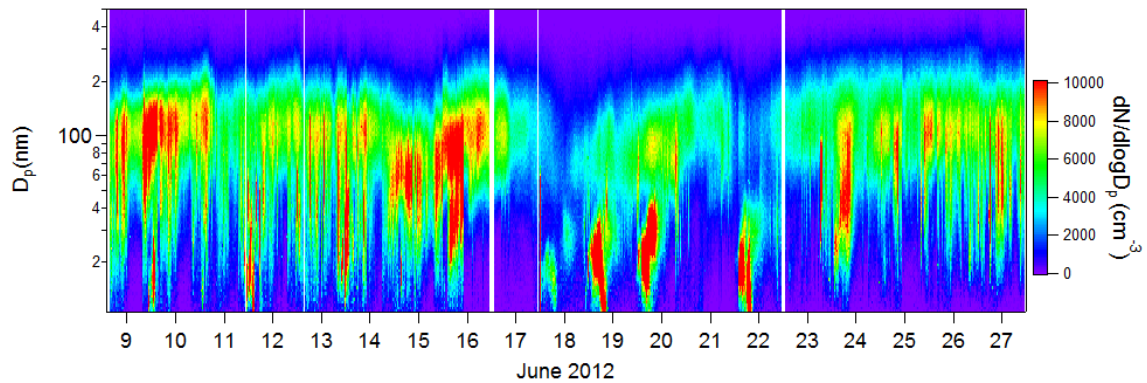


Figure 2. Size distributions at the ICE-HT area measured by an SMPS for the period between the 8th and the 27th of June 2012. No nucleation event was observed.

Positive matrix factorization (PMF) was applied to the high resolution (HR) organic aerosol mass spectra obtained by an Aerodyne High Resolution Aerosol Mass Spectrometer (HR-AMS) (Fig. 3). For Patras four sources could be identified: 18% LV-OOA (oxygenated OA of low volatility) related to aged OA, 60% SV-OOA (semi-volatile oxygenated OA) a less oxygenated OA, 14% COA (cooking OA) related to food preparation and 8% HOA (hydrocarbon-like OA) associated with traffic emissions (Fig 4.). In Athens again a 4-factor PMF solution was found to describe best the OA AMS: LV-OOA (36%), SV-OOA (31%), COA (16%) and HOA (17%). In both cities the major component was OOA, suggesting that under high photochemical conditions most of the OA in the Eastern Mediterranean is secondary.



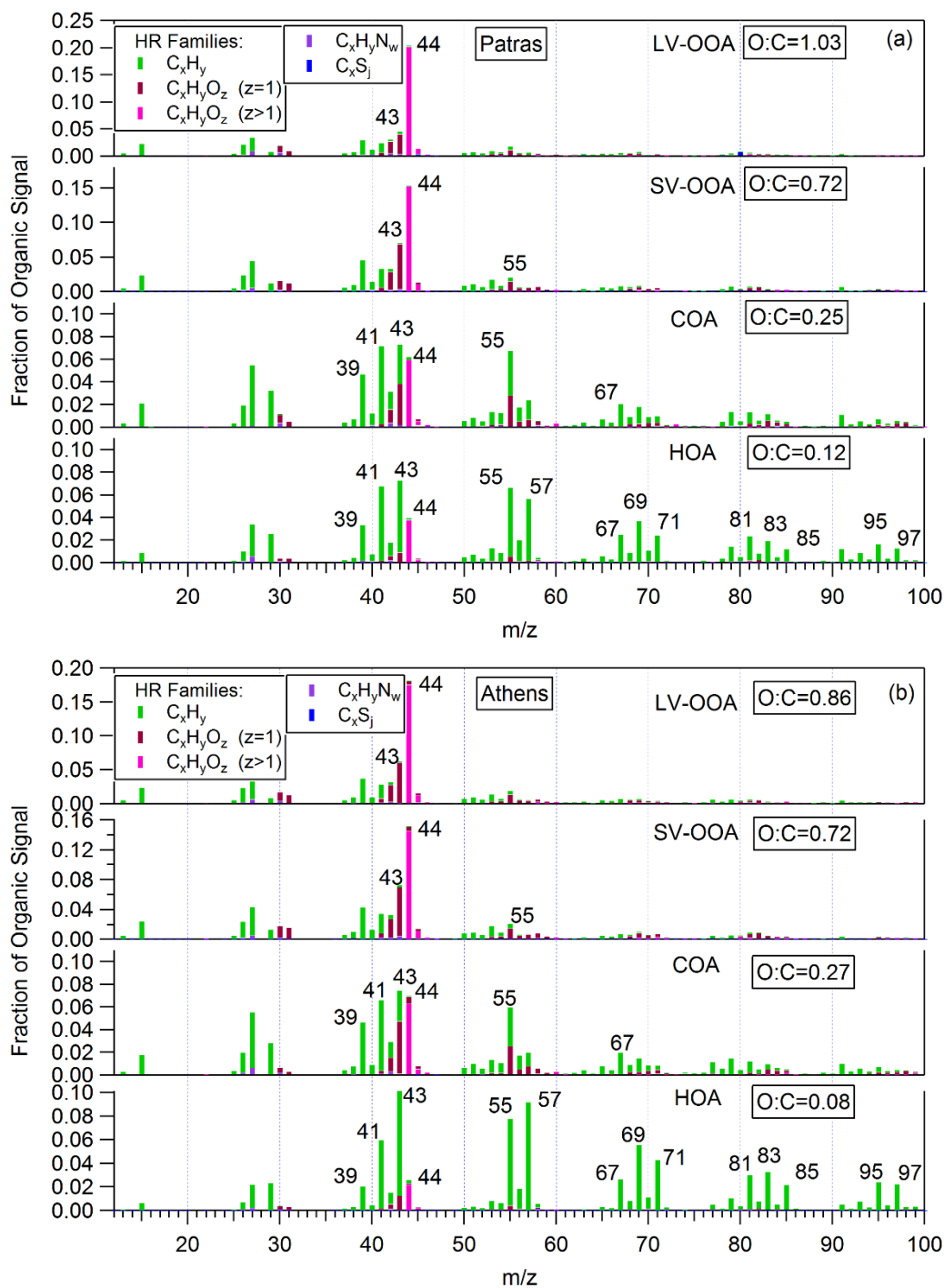


Figure 3. HR mass spectra profiles of the 4 sources found a) in Patras and b) in Athens.

The contribution of the primary sources (HOA and COA) was important (22% in Patras and 33% in Athens) but not dominant (Fig. 5).



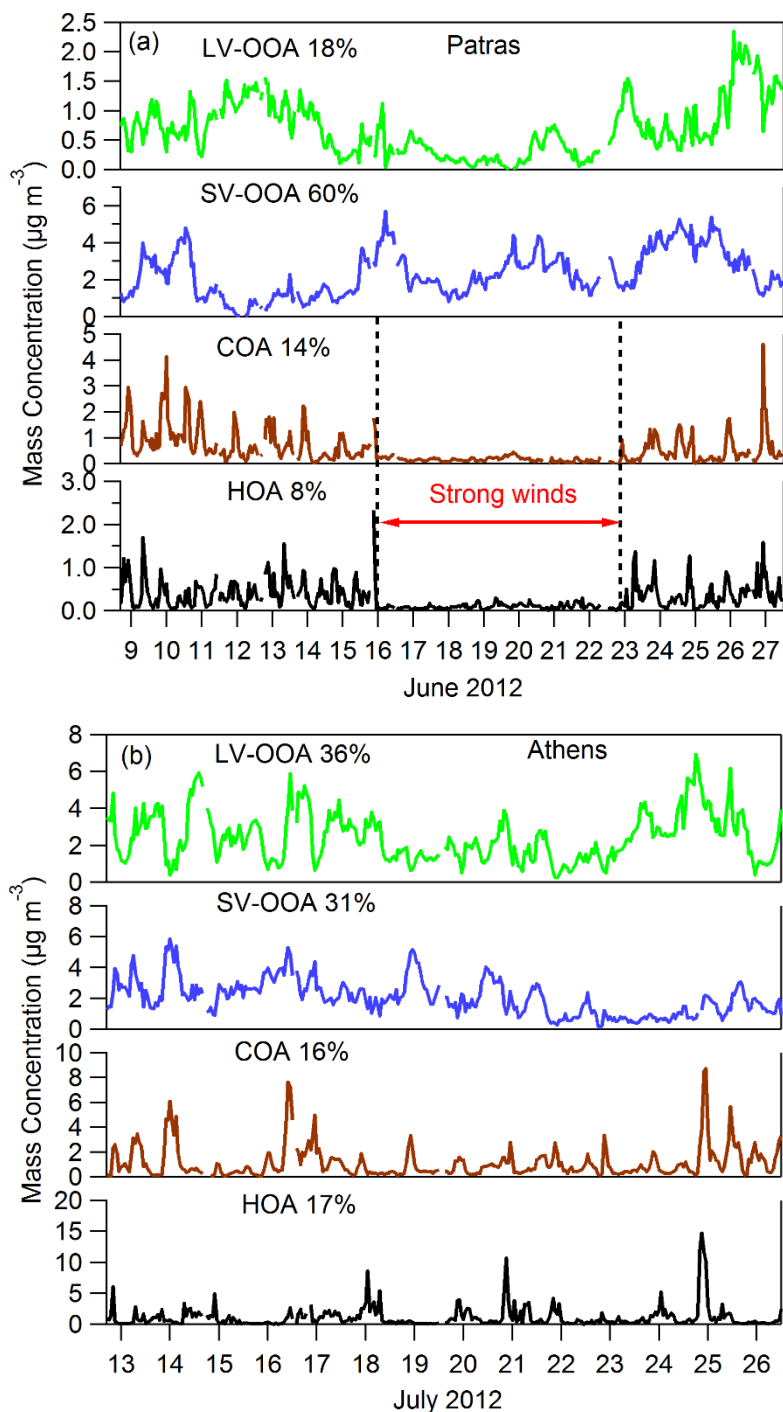


Figure 4. Time series a) of the 4 PMF factors using HR organic mass spectra for Patras and b) of the 4 PMF factors found in Athens. For the Patras measurements the HOA and COA contribution is almost eliminated between the 16th and 23rd of June 2012 due to the high wind speed during that period.

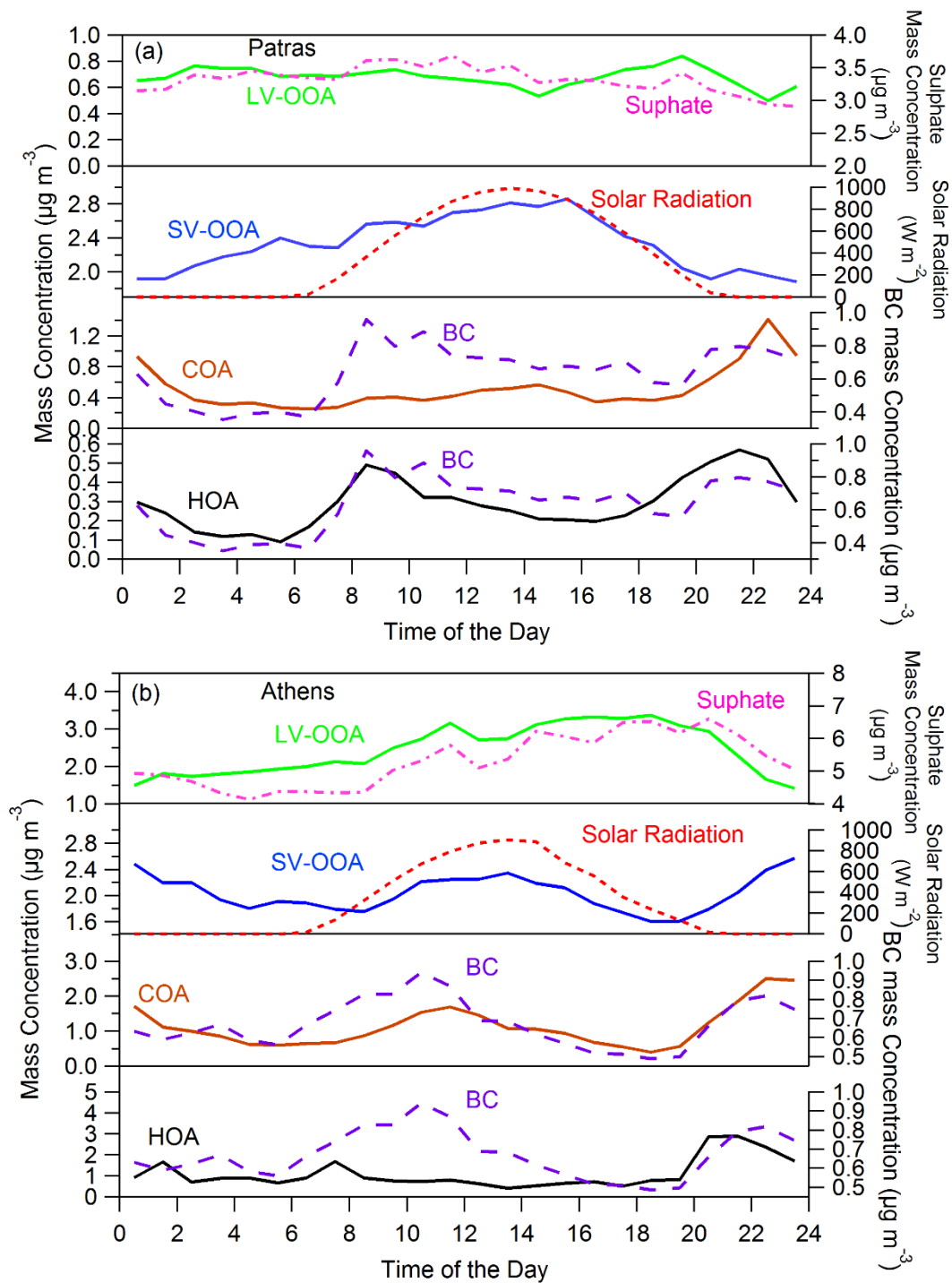


Figure 5. Diurnal cycles of the 4 PMF factors a) in Patras and b) in Athens.



Winter time air pollution in Patras

The sampling location was in the suburbs of the city of Patras (4 km away from the city centre) in the campus of Technological Educational Institute of Patras (TEI) ($38^{\circ}13'N$ $21^{\circ}45'E$) (Fig. 6). The measurements took place during the winter of 2012.

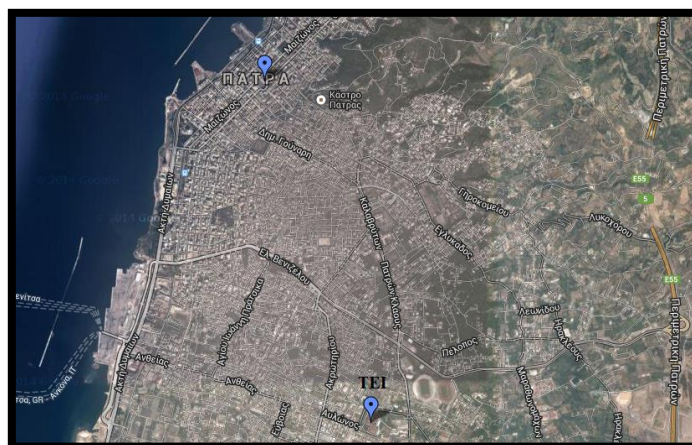


Figure 6. Location of sampling sites in the Technological Educational Institute (TEI). The center of Patra where the second station was located is also shown.

The instrumentation used in the TEI campus included an Aerodyne High-Resolution Time-of-Flight Mass Spectrometer (HR-ToF-AMS) and a selection of monitors such as an Aerodynamic Particle Sizer Spectrometer (APS), a Scanning Mobility Particle Sizer (SMPS, TSI 3936L) and a Tapered Element Oscillating Microbalances (TEOM), measuring on-line the aerosol size distribution. In addition, a filter sampler and a Multi-angle Absorption Photometer (MAAP) were deployed at the center of Patras (Fig. 6) at an elevation of approximately 20 m above sea level providing information about the spatial distribution of pollution (Fig. 7).





Figure 7. Left, the location of TEI in Patras. Right, the sampling site in the city centre (top of the the white building).

During the campaign, the ambient temperature ranged from 4⁰C to 15.7⁰C. The average temperature was 11⁰C and, as expected, was anti-correlated with relative humidity (RH) (Fig. 8).

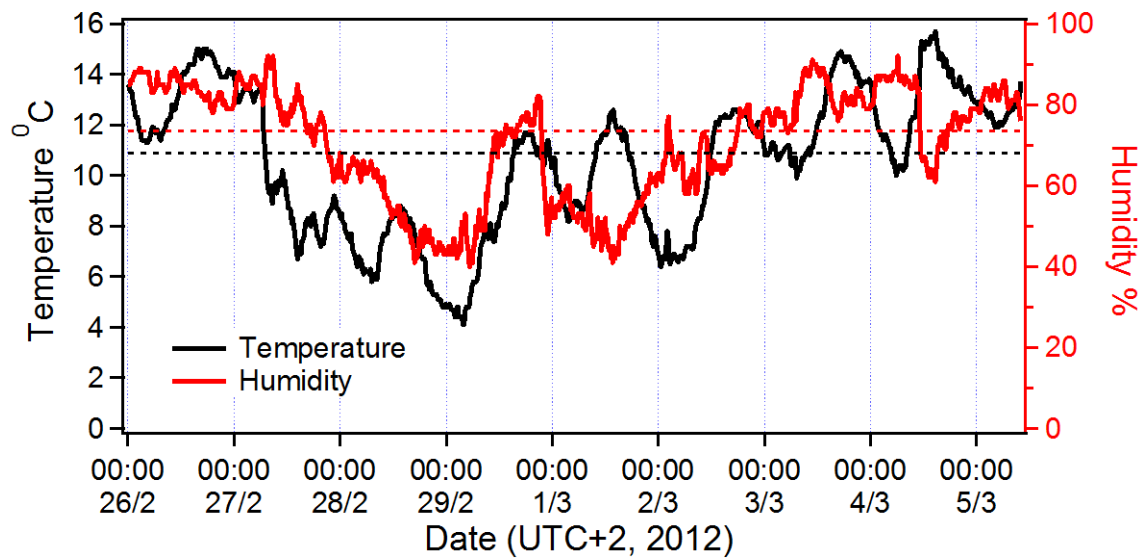


Figure 8 Temperature and relative humidity time-series during the campaign. The measurements were taken in Patras center.

 European Union European Social Fund	 OPERATIONAL PROGRAMME EDUCATION AND LIFELONG LEARNING <i>investing in knowledge society</i> MINISTRY OF EDUCATION & RELIGIOUS AFFAIRS MANAGING AUTHORITY	 NSRF 2007-2013 programme for development EUROPEAN SOCIAL FUND
Co-financed by Greece and the European Union		

In Fig. 9 the hourly total mass concentration of NR-PM₁ and the ambient temperature is shown. High PM₁ concentrations were observed during the evenings of February 29, March 2, 3 and 4.

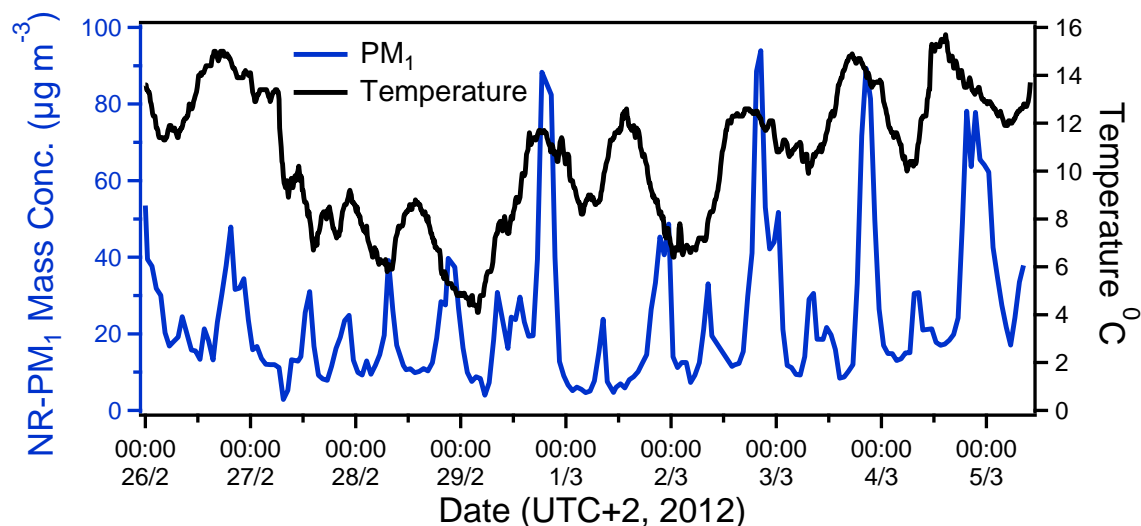


Figure 9. Total mass concentration NR-PM₁ in the TEI site and temperature during the campaign from Patras site.

The mass concentrations (in $\mu\text{g m}^{-3}$) of organic matter (OM), nitrate, sulphate, ammonium, chloride, and black carbon (from the MAAP) are shown, in Fig. 10. The MAAP was in the center of Patras, about 4 km away from the TEI location. The major component of PM₁ was organic matter which increased dramatically reaching levels up to $82 \mu\text{g m}^{-3}$ during the evening. The organic aerosol concentration also increased during morning rush hour, but the corresponding concentrations were less than $20 \mu\text{g m}^{-3}$. BC closely followed the trend of organic aerosol with maximum BC mass concentration of approximately $8 \mu\text{g m}^{-3}$ during nighttime and $4 \mu\text{g m}^{-3}$ during rush hour in the mornings. Nitrates followed a similar trend, but sulphate concentrations had smaller fluctuations during the campaign, indicating a different source origin.

In general, organic matter was the most abundant species (73% of PM₁) throughout the campaign, followed by sulphate, BC, ammonium and nitrate. The average composition of the main aerosol components is presented in Fig. 11.



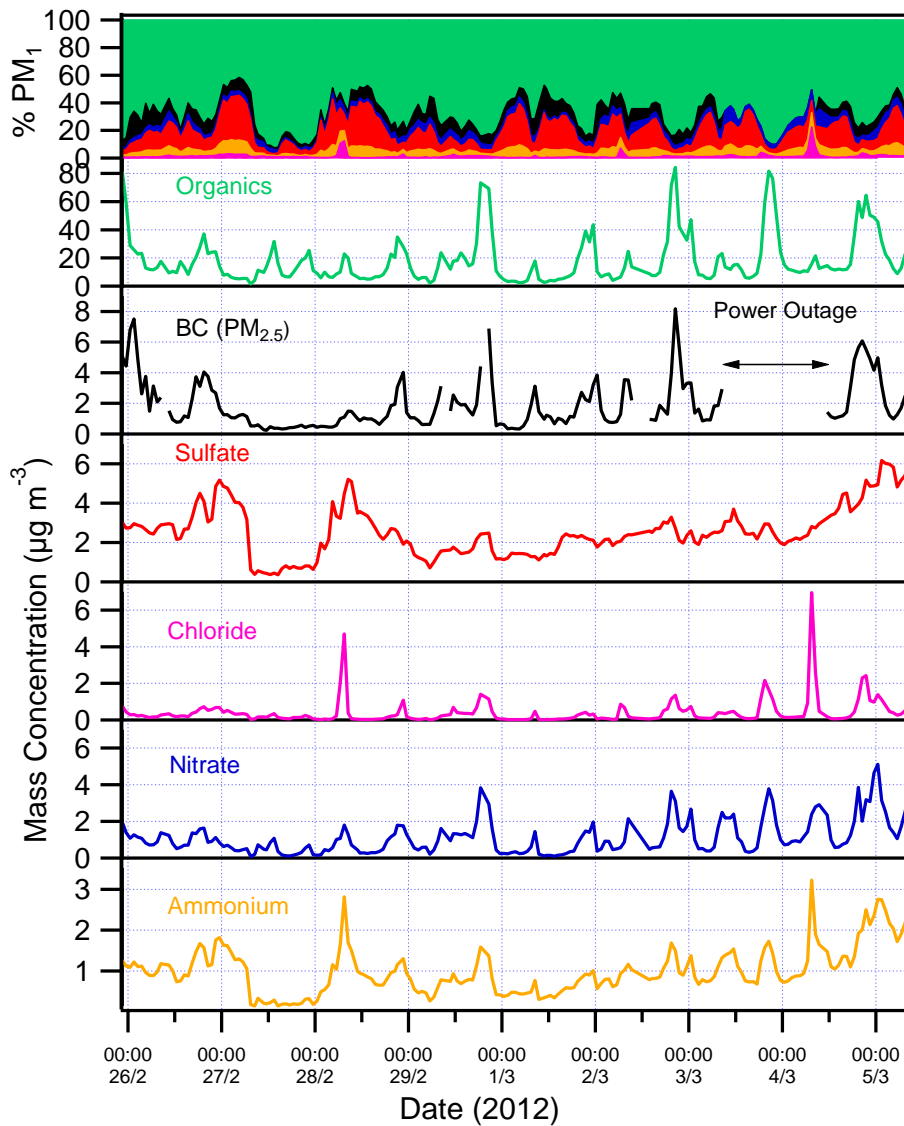


Figure 10. The hourly averaged PM_{10} composition by the HR-AMS at the TEI site and black carbon measurements of the same period at Patras center. Different scales are used for each species. Also, the contribution of each constituent of the dry PM_{10} mass is shown.



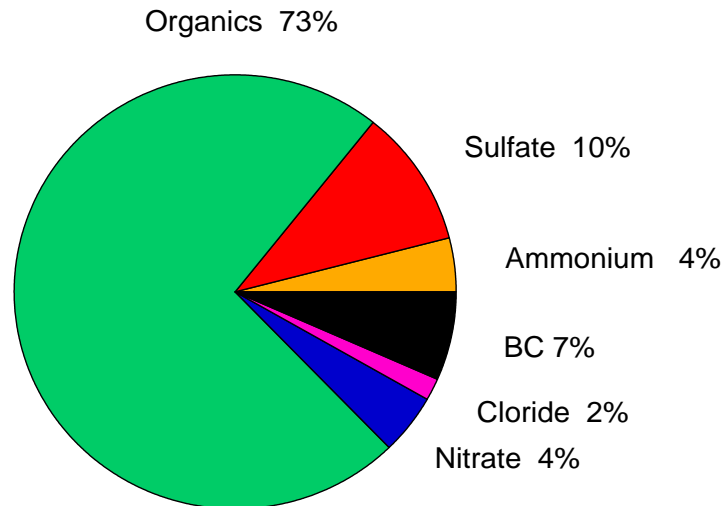


Figure 11. Average composition of PM_{10} during the 2012 campaign in Patras.

Figure 12 shows the average mass distributions for the ambient aerosol for the whole campaign. The modes of the different aerosol species (sulfate, organics, ammonium, chloride and nitrate) are at different diameters, implying that the PM_{10} particles during the sampling period had different composition at different size ranges.

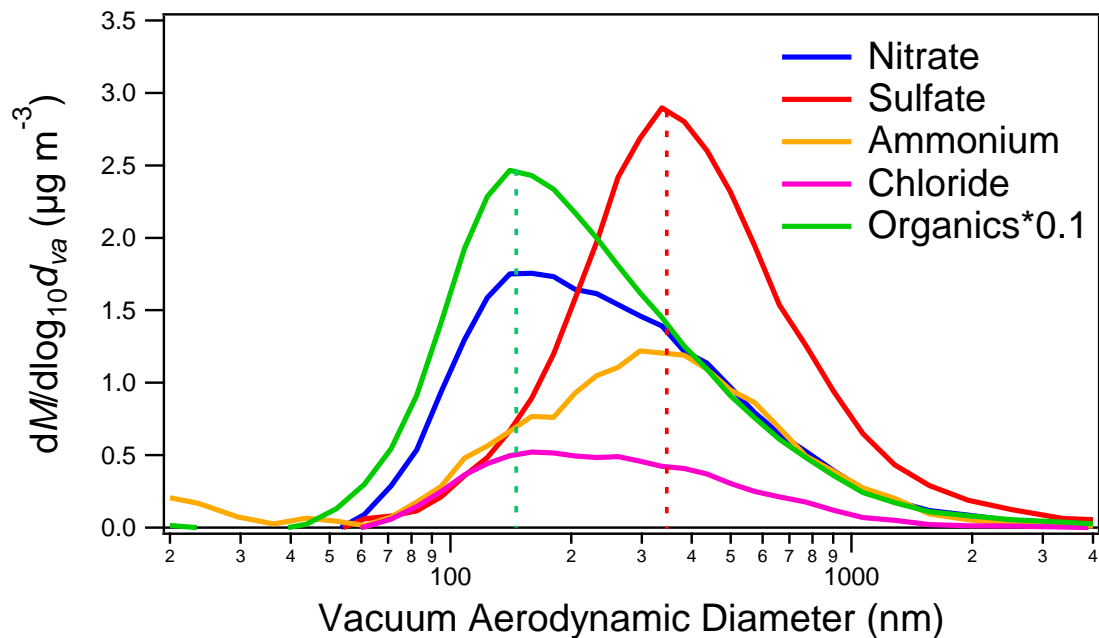


Figure 12. The campaign-average size distributions of the aerosol species measured by the AMS versus vacuum aerodynamic diameter.

 European Union European Social Fund	 OPERATIONAL PROGRAMME EDUCATION AND LIFELONG LEARNING <i>investing in knowledge society</i> MINISTRY OF EDUCATION & RELIGIOUS AFFAIRS MANAGING AUTHORITY	 NSRF 2007-2013 programme for development EUROPEAN SOCIAL FUND
Co-financed by Greece and the European Union		

The average diurnal profiles for the main NR-PM₁ species during the campaign are shown in Fig. 13. OM and BC show two significant peaks during the day. The first one appeared at around 8:00 am (Local Standard Time, LST), which coincides with the rush hour traffic and the second one at 19:00 in the evening. During the evening the OM and BC concentrations increased and were responsible for almost 90% of the total NR-PM₁ mass, until around midnight. Sulfate shows a rather flat profile during the day, while nitrate presents three peaks, of which two, coincide with those of OM and BC. This suggests that nitrates and OM had at least to some extent, similar sources.

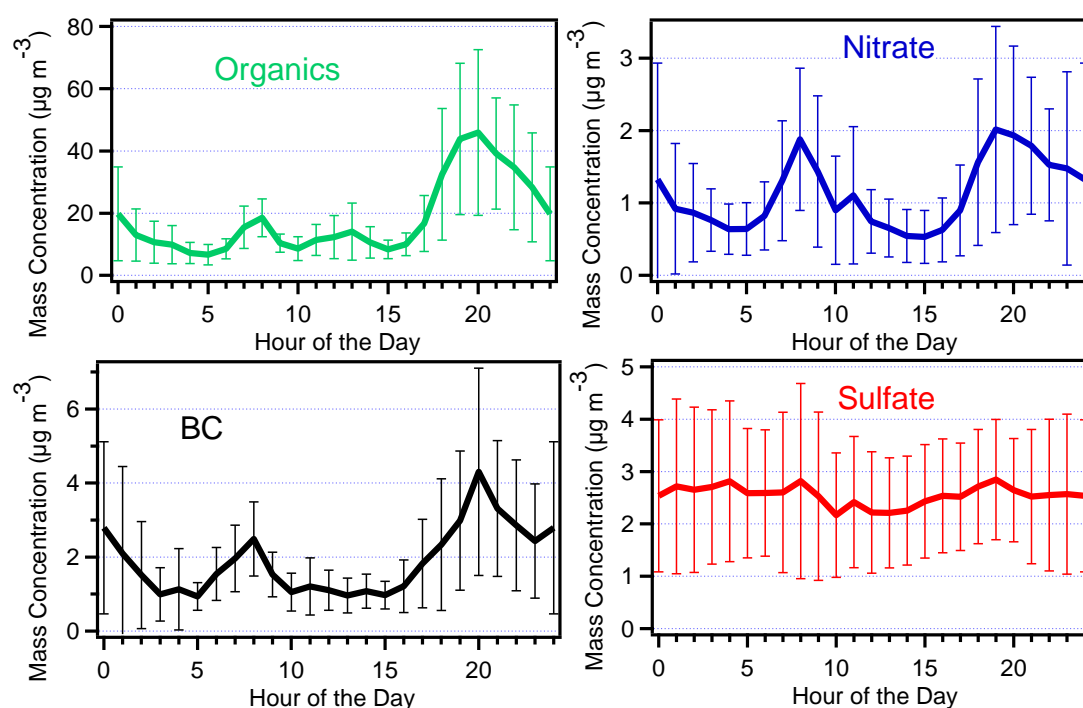


Figure 13. Average diurnal profiles of the concentrations of the major PM₁ components. The error bars correspond to one standard deviation of the measurements.

The average O/C ratio was low at 0.33 ± 0.07 and the H/C ratio high at 1.53 ± 0.05 . This is consistent with the organic aerosol being heavily dominated by primary emissions (Allan et al., 2010). The estimated N/C ratio (not shown here) was very low at 0.02 ± 0.003 .



Positive matrix factorization (Paatero and Tapper, 1994) was applied to the organic aerosol data, measured by the HR-ToF-AMS. The PMF analysis deconvoluted the organic aerosol spectra into four factors. The first one is a Biomass Burning Organic Aerosol (BBOA) factor and was responsible for 58% of the total OM mass during the campaign. It was followed by the Oxygenated Organic Aerosol (OOA) factor representing 18% of the total OM. This factor is generally attributed to aged OA transferred from other areas. The third and fourth factor are Hydrocarbon-like Organic Aerosol (HOA) and Cooking Organic Aerosol (COA) and are both attributed to freshly emitted OM from the combustion of fossil fuels (mainly traffic) or preparation of food, respectively. They both contributed to total OM approximately 12%. This solution has been evaluated through comparison of the corresponding spectra with literature spectra, the correlation between the factors and time-series of other pollutants, each factor's diurnal profile and their physical meaning (Zhang et al., 2005c; Ulbrich et al., 2009).

Figure 14 presents the hourly averaged time series of the four PMF factors and also their contribution to the total OM. The BBOA concentration increased during the evening reaching concentrations up to $65 \mu\text{g m}^{-3}$ around midnight and its hourly average value was $10.5 \mu\text{g m}^{-3}$.



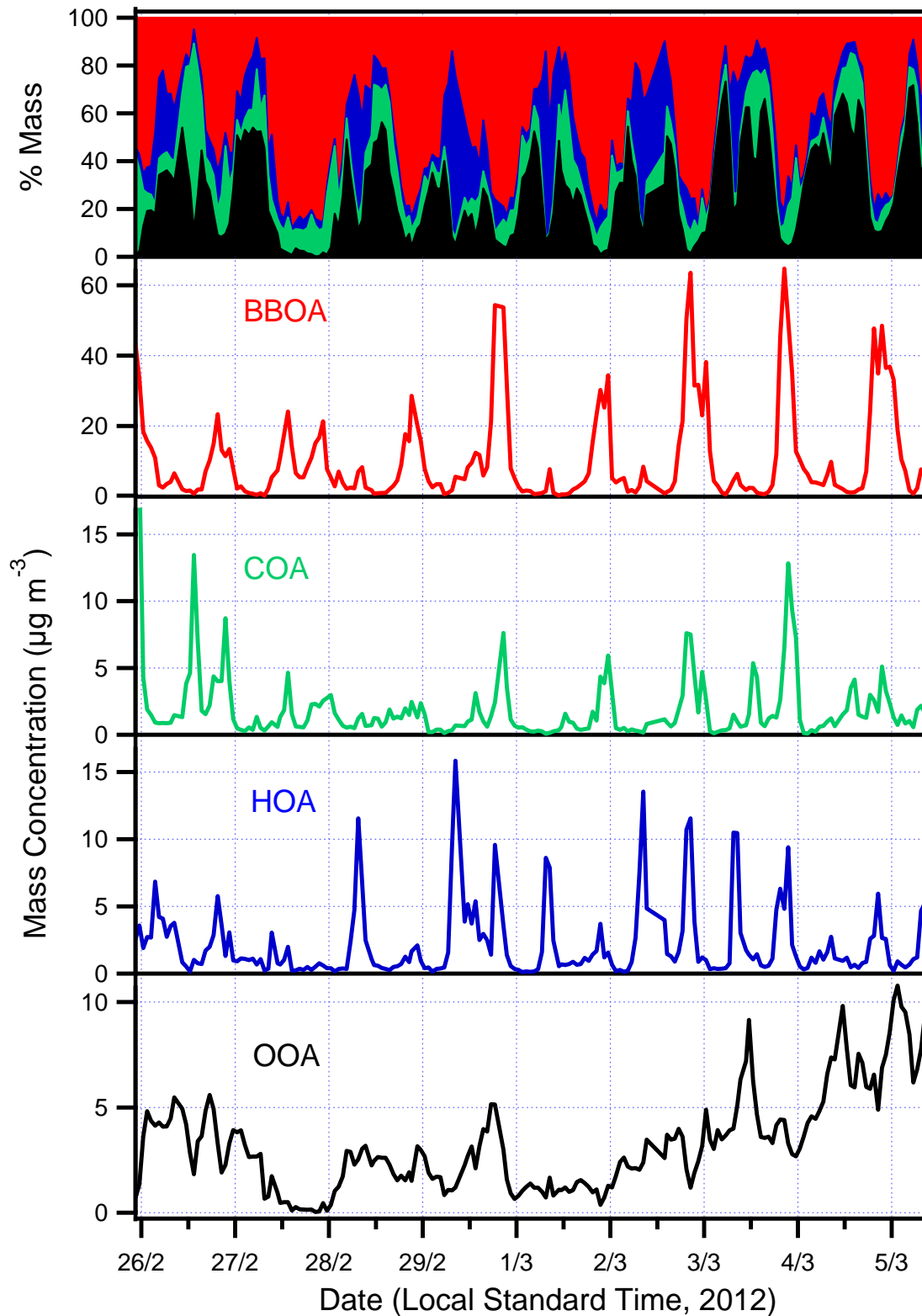


Figure 14. The concentration of PMF factors at the TEI site. Different scales are used for each factor. The contribution of each factor to total OM is shown (top figure).



The BBOA factor had the same trends as the total PM₁ with sharp increases after 16:00 pm (Local Standard Time, LST). The OOA factor dominated during the daytime. The OOA varied relatively slowly throughout the campaign and its hourly mean value was 3.2 $\mu\text{g m}^{-3}$ with a maximum value of 10.8 $\mu\text{g m}^{-3}$. The hourly mean value of the HOA factor was 2.1 $\mu\text{g m}^{-3}$ and of COA 2 $\mu\text{g m}^{-3}$. Their maximum hourly values were 15.8 $\mu\text{g m}^{-3}$ for HOA and 20 $\mu\text{g m}^{-3}$ for COA factor. The BBOA, HOA and COA factors correspond to primary sources, whereas the OOA factor to atmospheric processing (secondary OA). Figure 15 shows the mass spectra of the four OA components, identified by PMF for the entire campaign, which are similar to those reported in previous studies (Zhang et al., 2005c; Lanz et al., 2007; Nemitz et al., 2008; Ulbrich et al., 2009). Some m/z 's including 44, 57, and 60 are characteristic of OOA, HOA and BBOA, respectively. These factors are analyzed below.

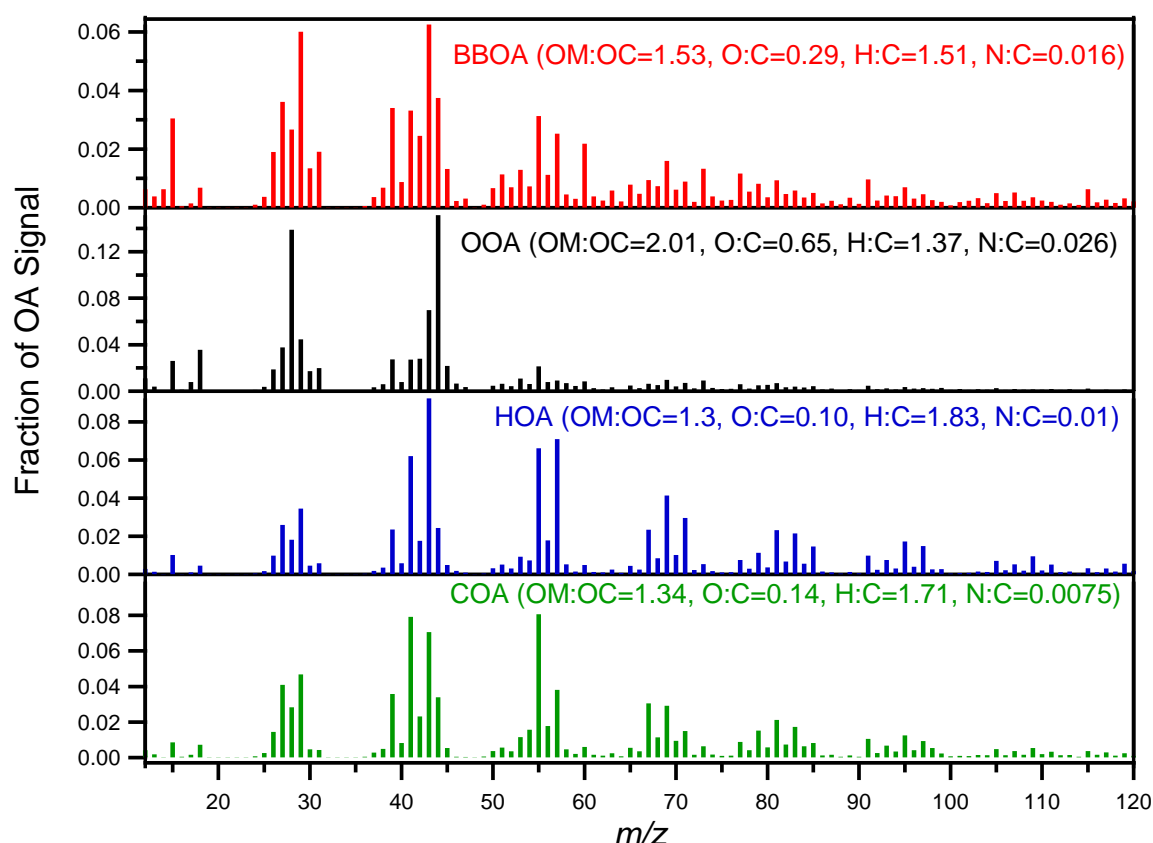


Figure 15. Mass spectra of the four OA factors with calculated corresponding atomic ratios.



Biomass Burning Organic Aerosol (BBOA): Typical mass fragments of the BBOA spectrum are m/z 60 and 73, attributed to $C_2H_4O_2^+$ and $C_3H_5O_2^+$, respectively. The BBOA factor correlates well with K^+ ($R^2=0.64$, Fig. 15), a biomass burning emission tracer. Its O:C ratio of 0.29 is higher than for the other primary sources (HOA and COA) and is consistent with the results of Alfarrá et al. (2004) and Aiken et al. (2009). BBOA in Patras originates from wood-combustion.

Oxygenated Organic Aerosol (OOA): OOA is a surrogate for secondary OA. Its spectrum is characterized a strong peak at m/z 44 (mostly due to CO_2^+) and a lower one at 43 (mostly due to $C_2H_3O^+$). It does not contain important contributions from marker peaks of other organic aerosol classes. The more the organic aerosol stays in the atmosphere, the more the fraction of m/z 44 (CO_2^+), increases (Ng et al., 2010). OOA represents the chemically aged OA and is mostly due to long range transport from other areas. The O:C ratio for OOA for this period was 0.65, consistent with other studies Zhang et al. (2011) and the OM:OC ratio was equal to 1.91. The OOA was correlated reasonably well with particulate ammonium ($R^2=0.61$) and sulfate ($R^2=0.56$). The correlation to nitrate was not as good ($R^2=0.4$).

Hydrocarbon-Like Organic Aerosol (HOA): HOA is characterized by ions with the general types $C_nH_{2n+1}^+$ and $C_nH_{2n-1}^+$. As a result, the HOA spectrum has characteristic peaks at m/z 41, 43, 55, 57, 69, 71, 83 and 85 etc., with little or no signal at 44. The largest peaks are at 43 ($C_3H_7^+$) and 57 ($C_4H_9^+$) (Fig. 4.14). The mass spectra of HOA are often similar to those of diesel exhaust (Canagaratna et al., 2004; Schneider et al., 2005), and other incomplete combustion sources. The HOA O:C elemental ratio is the lower one (0.1) while the H:C elemental ratio (1.83) is the highest among the PMF factors. The HOA correlation with BC was low ($R^2=0.2$) as the MAAP was monitoring 4 km away.

Cooking Organic Aerosol (COA): The COA spectrum has some similarity to that of HOA but is dominated by m/z 's 41 and 55 instead of 43 and 57 (Fig. 15). The COA spectra, like the HOA ones are characterized by the ion series: $C_nH_{2n+1}^+$ and $C_nH_{2n-1}^+$ but also by $C_mH_{2m-1}CO^+$ (m/z 41, 55, 69, 83...) and $C_mH_{2m+1}CO^+$ (m/z 29, 43, 57, 71, 85). The peak of COA concentrations coincide with typical meal times (Fig. 16). Its



O:C ratio, equal to 0.14 was low but higher than that of HOA. The COA H:C (1.71) was lower than the corresponding one of HOA. The average diurnal profile of the four factors is shown in Fig. 16. The BBOA peaks in the evening (maximum of $34 \mu\text{g m}^{-3}$, at 20:00 LST), which is consistent with residential heating. The OOA factor profile is relatively flat, a behavior expected of a pollutant transported to the receptor from other areas. These results are consistent with long term measurements in Patras that supported the importance of transported pollution as a major PM source throughout the year (Pikridas et al., 2013). The HOA factor has two major peaks during the day. Its major peak occurs in the morning (maximum of $7.2 \mu\text{g m}^{-3}$, at 20:00 LST) and coincides with the morning traffic. The second peak of HOA appeared in the early evening ($4.3 \mu\text{g m}^{-3}$, at 19:00 LST) and corresponds to the evening rush hour. COA's diurnal cycle exhibited a clearly different diurnal profile in comparison to HOA, with one peak in the late evening ($6.5 \mu\text{g m}^{-3}$, at 22:00 LST) and another one around midday ($4 \mu\text{g m}^{-3}$, at 13:00 LST) corresponding to mealtimes.

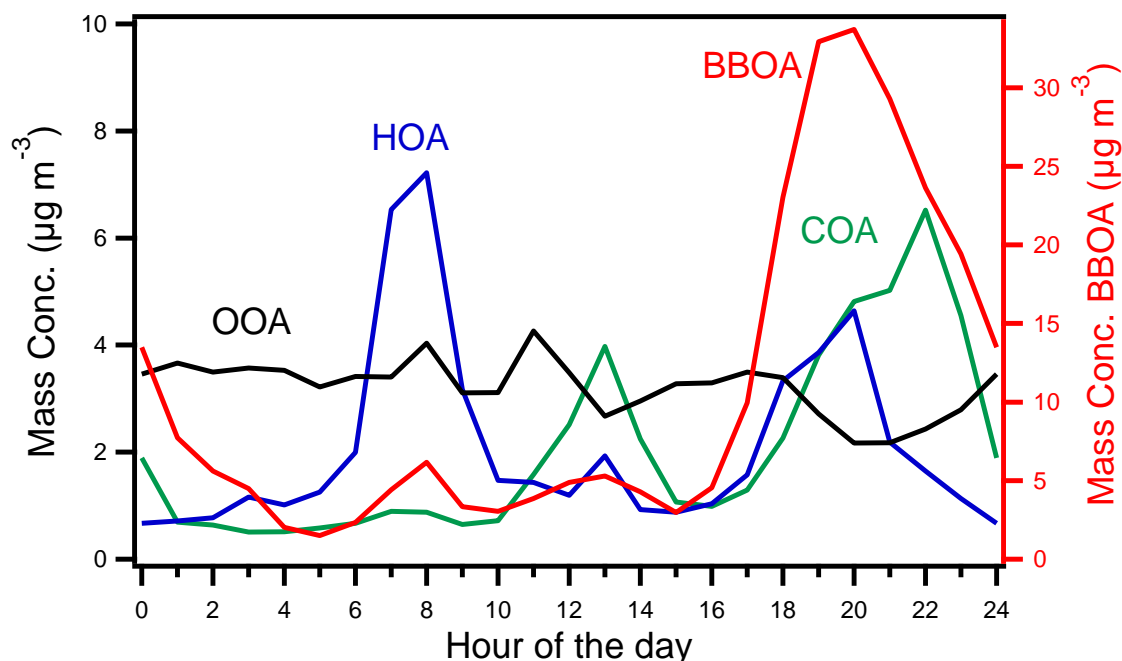


Figure 1 Average diurnal variation of the four PMF factors. The right y-axis shows the BBOA values, while the left one all the rest.



Activity D6

Vertically-resolved aerosol optical properties from satellite data

Cloud-Aerosol Lidar with Orthogonal Polarization (CALIOP) is an instrument aboard the Cloud-Aerosol Lidar and Infrared Pathfinder Satellite Observation (CALIPSO), designed to provide data on cloud and aerosols via active lidar techniques. We have used CALIOP Level 2-Version 3 Layer Aerosol Optical Depth (AOD) at 532 nm data, for a period of 3 complete years (2007-2009). These data are provided on a monthly, 5 km horizontal resolution and in up to 8 vertical layers. During Thales, the original CALIOP data have been regridded on a new horizontal ($2.5^{\circ} \times 2.5^{\circ}$) and vertical (40 layers) resolution. The regridding was performed so that the CALIOP data could function as input to a radiation transfer model, which will be presented later. The regridded CALIOP data is part of the vertically resolved AOD satellite database. From this database, we present 3-year sample vertical AOD profiles for Greece (Fig. 17a) and the Arabian Peninsula (Fig. 17b) analyzed for the four seasons.

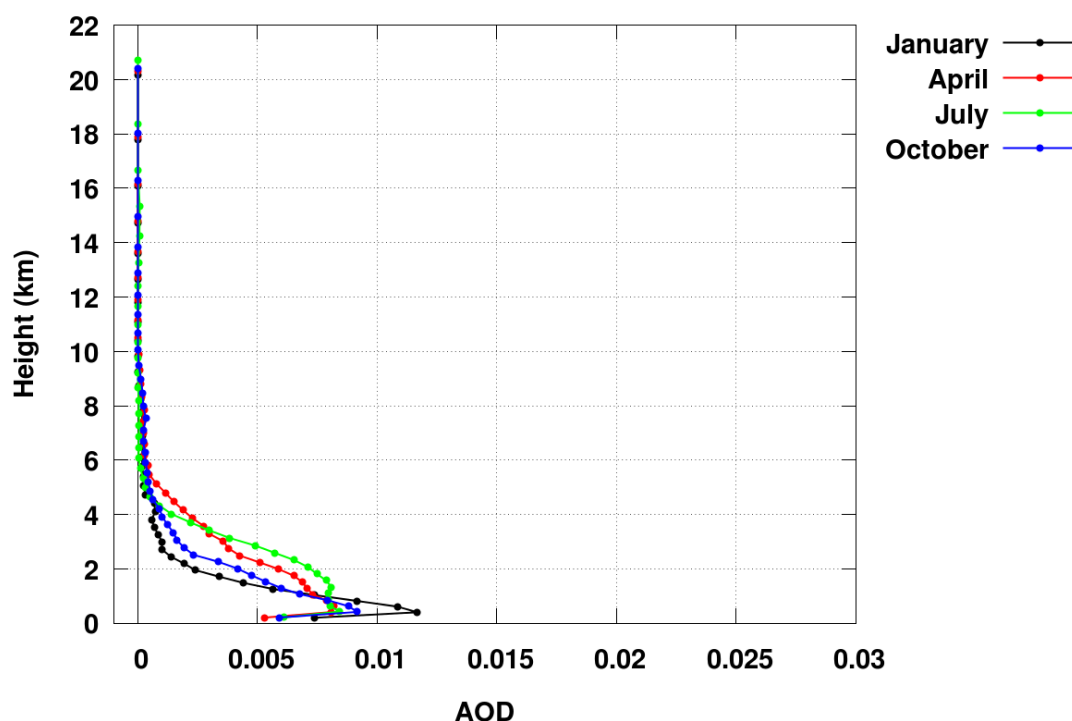


Figure 17a: 3-year (2007-2009) average of the vertically resolved AOD profile by CALIOP for the area of Greece. The four colored curves correspond to different seasons of the year.

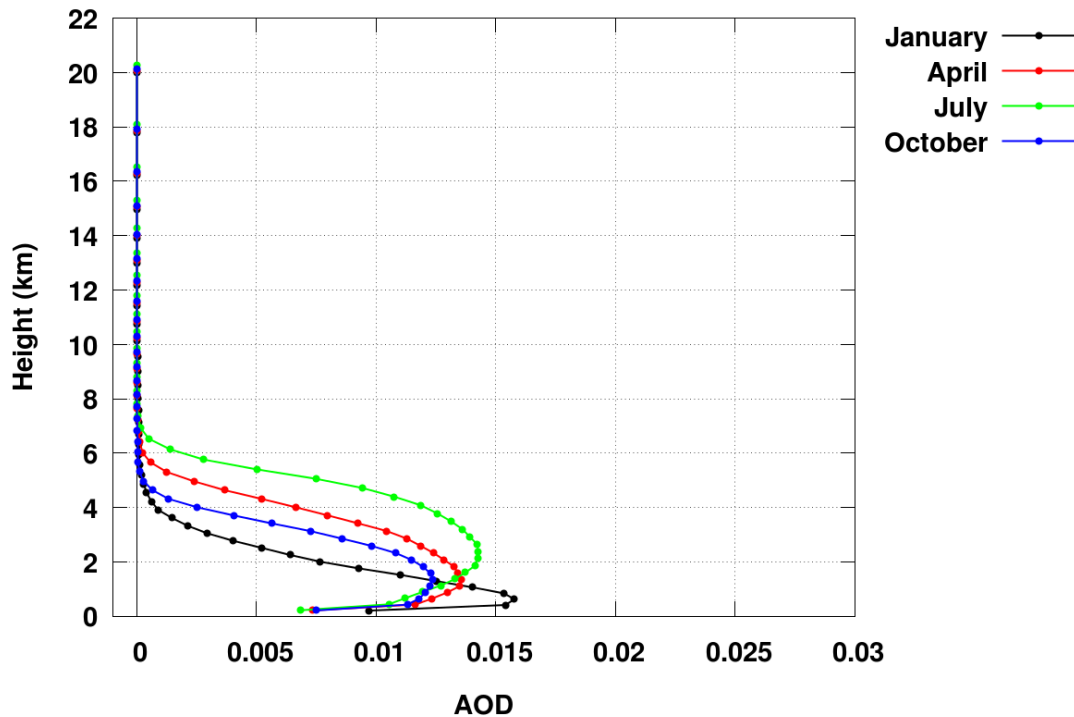


Figure 17b: Similar to Fig. 17a for the Arabian Peninsula

In both Figures 17(a) and (b), in the summer there is very little aerosol above 7 km from the surface, while the aerosol moves are confined under the height of 5 km in winter. Also, winter has the maximum AOD values at both locations. The Arabian Peninsula is characterized by larger AOD and larger load due to the existence of dust.

From the AOD database, we also present the 3-year average global map of columnar AOD (Fig. 18), where well-known aerosol-laden areas are prominent, e.g. the Sahara and Arabian deserts, Southeast Asia, Central Africa, the Amazon basin, the tropical Atlantic. This map generally corroborates the validity of CALIOP AOD data, even though the Sahara values are biased low.



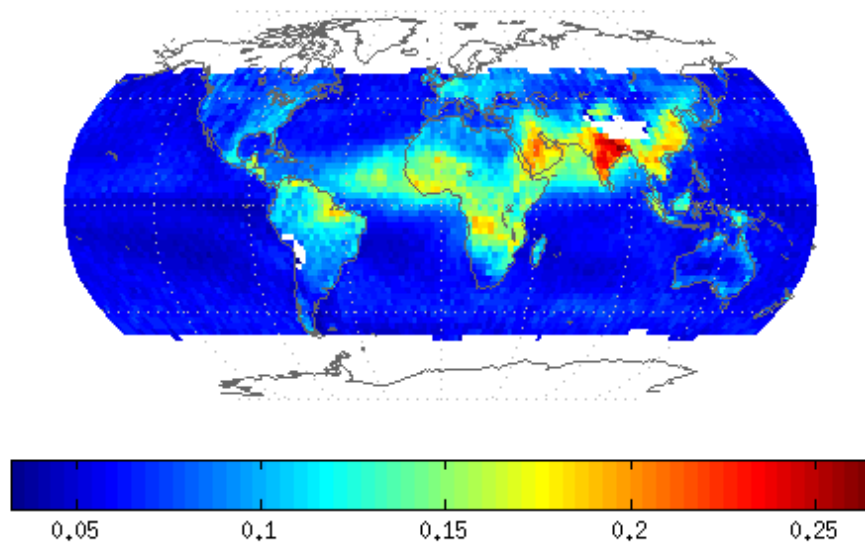


Figure 18: 3-year (2007-2009) CALIOP columnar AOD for the globe

Our database is complemented with some extra data sources: Detailed spectral resolution of aerosol optical properties (optical depth, asymmetry parameter and single scattering albedo) are provided by the Global Aerosol Data Set (GADS, Koepke et al., 1997). Cloud data (cloud amount, optical depth and top pressure) given for 15 cloud types (low, middle and high) are taken from the International Satellite Cloud Climatology Project (ISCCP, Rossow and Schiffer, 1999). The model input data include also vertical temperature and humidity profiles (from NCEP/NCAR global reanalysis project, Kistler et al., 2001), surface albedo and ozone concentration (from TIROS Operational Vertical Sounder).



Aerosol optical properties from PMCAMx-2008 and AtmOpt

The PMCAMx-2008 chemical transport model output is well suited for calculations of the aerosol optical properties. PMCAMx-2008 provides size-resolved chemical composition concentrations, for aerosol particles with diameters ranging from 0.04 to 40 μm , using 10 size bins (Table-I). The aforementioned output above is provided as gridded three-dimensional data, using 14 vertical layers, reaching up to the height of approximately 6 km. Inorganic aerosol growth, including water uptake due to hygroscopic growth of the particles, at increased humidities, is calculated using the thermodynamic equilibrium model ISORROPIA (Nenes et al., 1998). PMCAMx-2008 also incorporates a detailed module for simulating the secondary organic aerosol (SOA) formation and growth (Koo et al., 2003).

Table-I. PMCAMx – 2008 aerosol size bins

Size Bin	Diameters range (μm)
1	0.039063 – 0.078125
2	0.078125 – 0.15625
3	0.15625 – 0.3125
4	0.3125 – 0.625
5	0.625 – 1.25
6	1.25 – 2.5
7	2.5 – 5.0
8	5.0 – 10.0
9	10.0-20.0
10	20.0-40.0

Taking into account all vertical layers, and assuming that the aerosol contribution to the total atmospheric scattering and absorption, above 6.0 km, is negligible, we can estimate a variety of critical aerosol optical properties. AtmOpt was specifically built for the purpose of post-processing the PMCAMx output and acting as an intermediate platform that unifies different models and observational datasets. AtmOpt provides AOD, scattering, absorption, and asymmetry parameter predictions (AOD_P) at 13 discrete wavelengths ($\lambda = 0.2, 0.3, 0.44, 0.55, 0.65, 0.80, 1.0, 1.2, 1.5, 2.0, 2.5, 3.0$ and $4.0 \mu\text{m}$). AOD values are the sum of all the partial AODs at each layer ($i = 1, \dots, 14$):

$$\text{AOD}_P(\lambda) = \sum_{i=1}^{14} b_{ext,i}(\lambda) \Delta z_i$$



$b_{\text{ext},i}(\lambda)$ being the layer i specific extinction coefficient equal to the sum of scattering and absorption coefficients, and Δz_i being the layer thickness.

When we have a variety of aerosol chemical species with known densities and wavelength-dependent complex refractive indices, the homogeneous sphere complex refractive index is calculated as the volume-weighted average of the individual refractive indices (Piliinis and Pandis, 1995). After reviewing the available literature, the reference datasets of the complex refractive indices, were assumed based on the field of application (Table-II).

Table-II. Assumed complex refractive indices per chemical.

Chemical Component	wl Range (μm)	Real RI 550nm	atImag. RI 550nm	at Comments
SO ₄ , NH ₄	0.2 – 40.0	1.53	1.0×10^{-7}	Ammonium sulphate /GEISA-2011 and GACP (NASA) Datasets
NO ₃	0.2 – 5.0	1.556	1.1×10^{-9}	Ammonium nitrate /GACP dataset
Cl and Na	0.2 – 40.0	1.5	1.0×10^{-8}	Sea salt/GACP dataset
OC	Not available	1.5	0.	Keep this value fixed at all wl
EC	0.2 – 40.0	1.75	4.4×10^{-1}	Soot /GEISA-2011 database
CRST	0.2 – 40.0	1.53	5.5×10^{-3}	Minerals / GEISA-2011 database

In similar studies the aerosol extinction coefficients are calculated using two principal approximations. In some cases Mie theory is applied for dry aerosol particles, along with pre-defined hygroscopic growth functions (Chin et al., 2002; 2003; Kinne et al., 2003). Other studies make use of the simplified “reconstructed extinction coefficient” method (Roy et al., 2003; Song et al., 2008, Han et al., 2010; Park et al., 2011, Li et al., 2012), introduced by Malm et al., (1994; 2000). The latter approach also makes use of



hygroscopic growth functions. These methods are (i) unsuitable for taking full advantage of the detailed PMCAMx – 2008 output and (ii) do not provide calculations of the full set of the aerosol optical properties (e.g. asymmetry parameter). PMCAMX-2008 dynamically tracks the size evolution of the aerosol mass. As a result, in this study, aerosol extinction is calculated without making any pre-assumptions regarding the aerosol size distribution and hygroscopic growth. To do so we implement standard Mie code, that takes into account the chemically and size resolved aerosol profiles, including aerosol water concentrations. Fig. 19 presents the spatial distribution of the key aerosol optical properties output of the AtmOpt modular system.



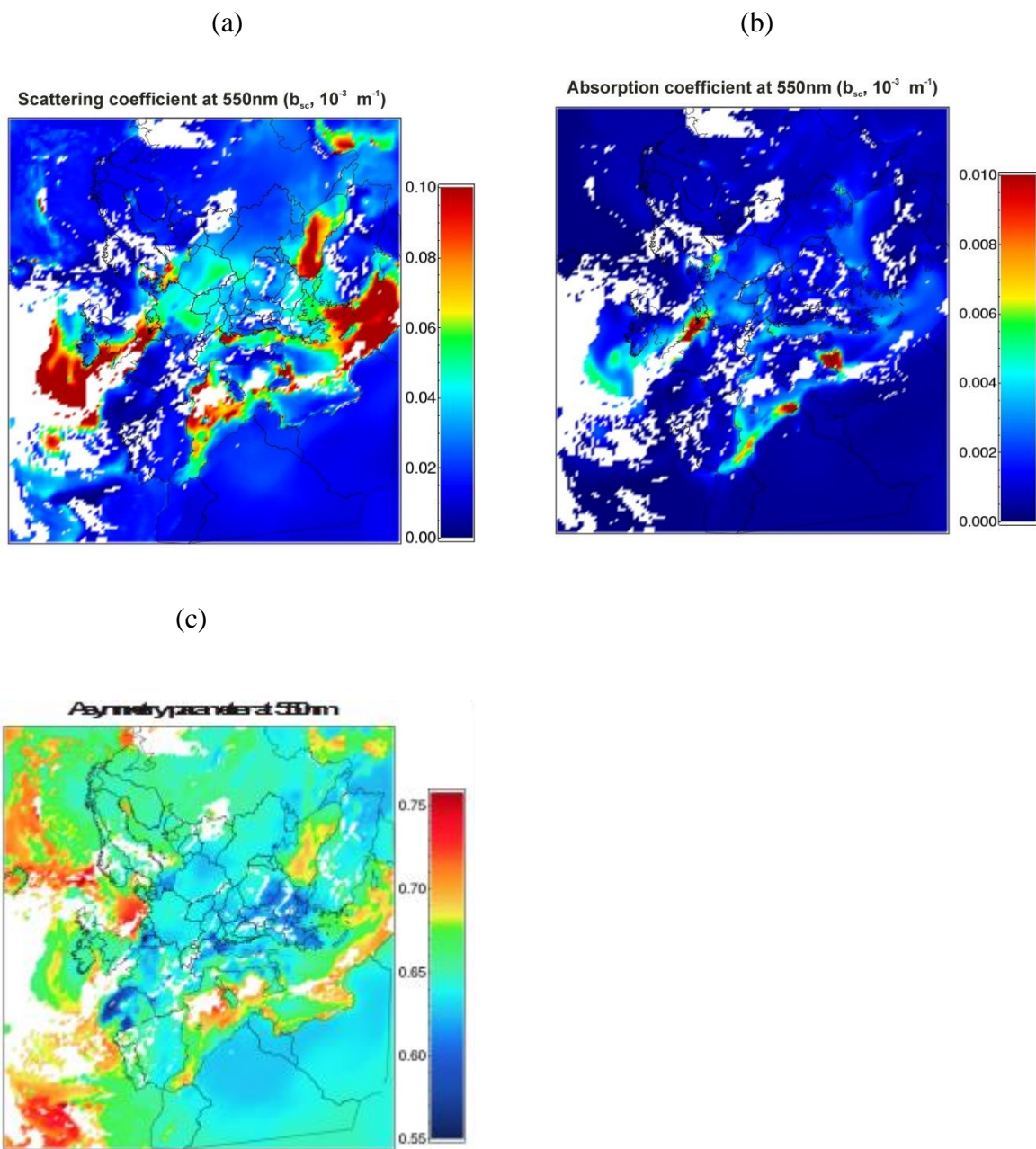


Figure 19: Hourly aerosol scattering coefficient (a), absorption coefficient (b) and asymmetry parameter (c) at 550 nm over Europe. Illustrations are examples of the AtmOpt output at ground layer and for May 15th 2008 – 12:00.



FORTH radiation transfer model results

The spectral radiative transfer model FORTH (Vardavas and Carver, 1984; Hatzianastassiou et al., 2004a; 2007a, b; Vardavas and Taylor, 2011) computes solar radiative fluxes at 118 wavelengths in the range 0.2–1.0 μm and 10 spectral intervals in the range 1.0–10 μm . The computations are performed for each 2.5° latitude x 2.5° longitude cell of the region under clear- or cloudy-sky conditions, considering ozone absorption, Rayleigh scattering, and absorption by water vapor, carbon dioxide and methane. Scattering and absorption by clouds (low, middle and high) and aerosols, and reflection from the Earth's surface are also taken into account. A complete description and detailed model considerations can be found in previous publications (Hatzianastassiou and Vardavas, 1999; 2001; Hatzianastassiou et al., 2004a, b, c, 2005; Hatzianastassiou et al., 2007a). The aerosol direct radiative effect (DRE) is computed as the difference between model-computed fluxes with (F_i) and without ($F_{i,\text{no-aerosol}}$) the presence of aerosols:

$$\text{DRE}_{\text{atm}} = F_{\text{atm}} - F_{\text{atm,no-aerosol}}$$

$$\text{DRE}_{\text{surf}} = F_{\text{surf}} - F_{\text{surf,no-aerosol}}$$

$$\text{DRE}_{\text{TOA}} = F_{\text{TOA,no-aerosol}} - F_{\text{TOA}}$$

The DRE components quantify the effect of aerosols on the net solar radiation at the top of atmosphere (TOA), DRE_{TOA} , on the absorbed radiation within the atmosphere, DRE_{atm} , and on the net downward or absorbed radiation, DRE_{surf} at the Earth's surface.

The FORTH model can be driven with two sets of aerosol optical properties, a) with the database from the vertically-resolved satellite measurements (e.g. AOD from CALIOP) and b) with the optical properties output of AtmOpt. In the case of a) the model is run globally in all-sky mode with a coarse resolution (monthly 2.5°x2.5°), while the case of b) the cloudy areas are left out and the model runs in clear-sky mode



over Europe with a finer resolution (hourly, 36 km x 36 km). Other than the aforementioned differences, the radiation transfer model runs essentially similarly and independently for (a) and (b).

Results of the run with CALIOP AOD are shown in Fig. 20a and Fig. 20b with the direct radiative effect of aerosols in the atmospheric column and at the surface absorbed radiative flux, respectively. At locations with large AOD, as expected the atmosphere is heated substantially (large positive values in Fig. 20a, especially if the aerosol is absorptive). The surface is cooled wherever large AOD values are found (negative values in Fig. 20b).

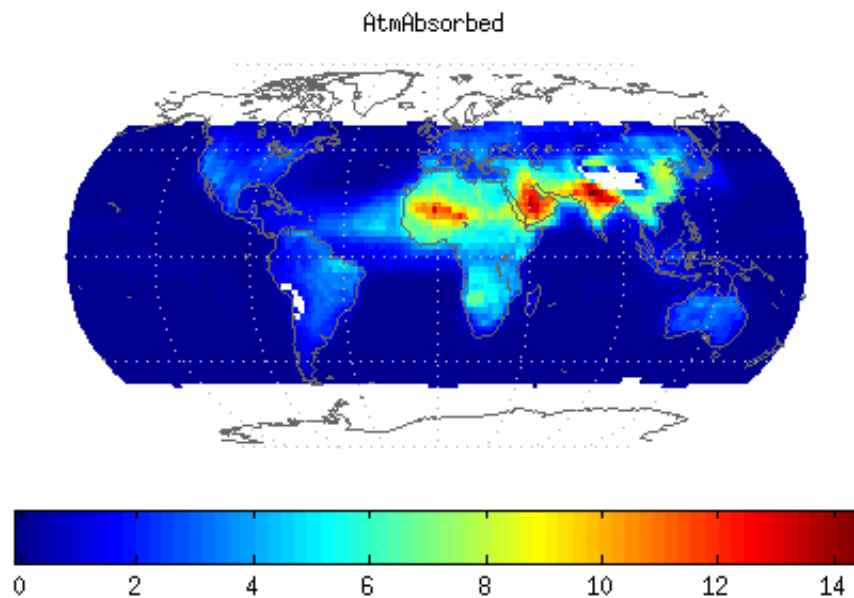


Figure 20a: 3-year (2007-2009) direct aerosol radiative effect (in Wm^{-2}) in the atmospheric column, as given by CALIOP AOD input to the radiation transfer model FORTH

 European Union European Social Fund	 OPERATIONAL PROGRAMME EDUCATION AND LIFELONG LEARNING <i>investing in knowledge society</i> MINISTRY OF EDUCATION & RELIGIOUS AFFAIRS MANAGING AUTHORITY	 NSRF 2007-2013 programme for development EUROPEAN SOCIAL FUND
Co-financed by Greece and the European Union		

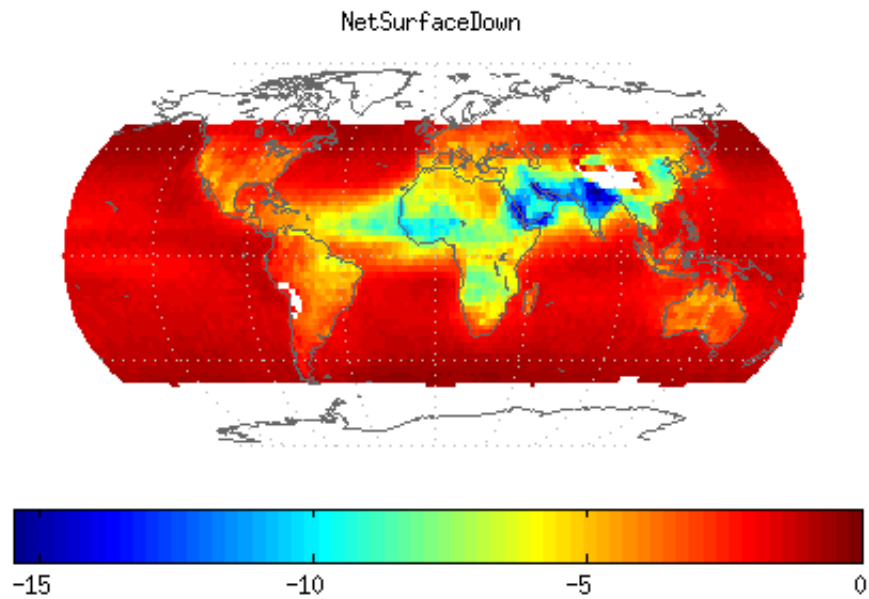


Figure 20b: Similar to Fig. 20a but for the radiative effect on the absorbed radiative flux at the surface

The DRE values at the top of the atmosphere, atmospheric column and at the surface can also be derived from the case b) run with the data produced by *AtmOpt* over Europe. For example, Fig. 21a highlights the aerosol-induced TOA cooling over areas with large AOD. There are also instances where the TOA DRE is positive, but this is always linked to large surface albedo, e.g. in snow-covered parts of Scandinavia and Alps, and reflective parts of Sahara. On the other hand, values in Fig. 21b are always negative, showing that aerosol acts as a cooling agent for the planetary surface, and even more so when AOD values are large and surface albedo is small.

 European Union European Social Fund	 OPERATIONAL PROGRAMME EDUCATION AND LIFELONG LEARNING <i>investing in knowledge society</i> MINISTRY OF EDUCATION & RELIGIOUS AFFAIRS MANAGING AUTHORITY	 NSRF 2007-2013 programme for development EUROPEAN SOCIAL FUND
Co-financed by Greece and the European Union		

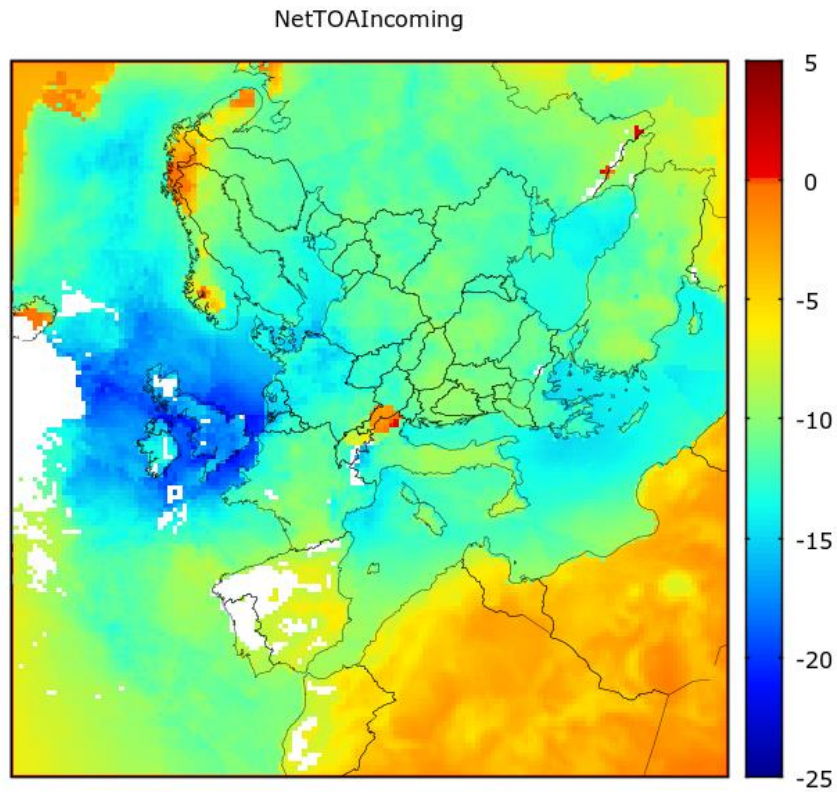


Figure 21a: Direct aerosol radiative effect at the TOA over Europe, produced by AtmOpt aerosol optical properties input in FORTH

 European Union European Social Fund	 OPERATIONAL PROGRAMME EDUCATION AND LIFELONG LEARNING <i>investing in knowledge society</i> MINISTRY OF EDUCATION & RELIGIOUS AFFAIRS MANAGING AUTHORITY	 NSRF 2007-2013 <small>programme for development</small> EUROPEAN SOCIAL FUND
Co-financed by Greece and the European Union		

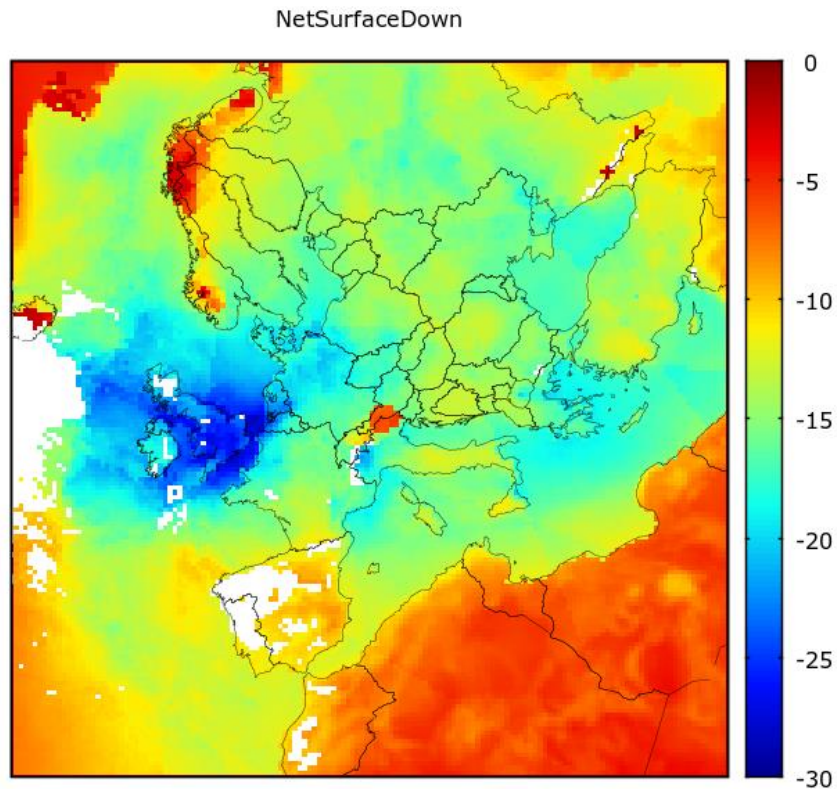


Figure 21b: Similar to Fig. 21a, but for the absorbed radiation flux at the surface

PUBLICITY-PUBLICATIONS

This program is so far highly successful in terms of publicity. Apart from the workshop mentioned above, the experimental campaign revealed new information regarding the contribution of fireplaces in air quality, which attracted the media and a press conference at IANOS that was later presented in the central news of major TV channels.

Since the First Progress Report, a number of articles have been prepared and presented in major conferences:

- Liakakou E., Stavroulas J., Roukounakis N., Psiloglou V., Fourtziou L., Paraskevopoulou D., Sciare J., Gerasopoulos E., Mihalopoulos N. “Black



carbon measurements during winter 2013-2014 in Athens and intercomparison between different techniques”, EGU2014, Vienna, Austria.

- Gerasopoulos, E., E. Liakakou, V. Psiloglou, J. Stavroulas, L., Fourtziou, N. Roukounakis, M. Lianou, N, Kappos, P. Zarmpas, H. Kambezidis, J. Sciare, N. Mihalopoulos, “Smog events over Athens during winter 2013-2014: Pollution measurements and chemical characterization” , EGU2014, Vienna, Austria.
- Gkikas A., N. Hatzianastassiou and N. Mihalopoulos “Characterization of intense aerosol episodes in the Mediterranean basin from satellite observations”, EGU2014, Vienna, Austria.
- Korras-Carraca M. B., V. Pappas, C. Matsoukas, N. Hatzianastassiou and I. Vardavas, “Global profiles of the direct aerosol effect using vertically resolved aerosol data” , EGU2014, Vienna, Austria.
- Pappas V., Hatzianastassiou N., Matsoukas C., Vardavas I. “Sensitivity of the atmospheric heating/cooling rate profile to the vertical distribution of aerosols”, COMECAP 2014, Heraklion, Greece.
- Korras-Carraca M. B., Pappas V., Matsoukas C., Hatzianastassiou N., Vardavas I. “Aerosol effect on atmospheric heating rate profiles using vertically resolved satellite aerosol data”, COMECAP 2014, Heraklion, Greece.

References

Chin, M., Ginoux, P., Kinne, S., Torres, O., Holben, B. N., Duncan, B. N., Martin, R. V., Logan, J. A., Higurashi, A., and Nakajima, T. (2002). Tropospheric aerosol optical thickness from the GOCART model and comparisons with satellite and sunphotometer measurements, *J. Atmos. Sci.*, 59, pp. 461–483



Chin, M., Chu, A., Levy, R., Remer, L., Kaufman, Y., Holben, B., Eck, T., Ginoux, P., and Gao, Q., (2003), “Aerosol distribution in the Northern Hemisphere during ACE-Asia: Results from global model, satellite observations, and Sun photometer measurements”, *J. Geophys. Res.*, 109, D23S90, doi:10.1029/2004JD004829

Han X., Zhang M. G., Han Z. W., Xin J. Y., Wang L. L., Qiu J. H. and Liu Y. J. (2010). Model analysis of aerosol optical depth distributions over East Asia, *53(7)*, pp. 1079-1090, doi: 10.1007/s11430-010-3079-z

Hatzianastassiou, N., Katsoulis, B., and Vardavas, I., (2004), “Global distribution of aerosol direct radiative forcing in the ultraviolet and visible arising under clear skies”, *Tellus*, 56B, 51–71

Hatzianastassiou, N., Matsoukas, C., Drakakis, E., Stackhouse Jr., P. W., Koepke, P., Fotiadi, A., Pavlakis, K. G., and Vardavas, I., (2007a), ”The direct effect of aerosols on solar radiation based on satellite observations, reanalysis datasets, and spectral aerosol optical properties from Global Aerosol Data Set (GADS)”, *Atmos. Chem. Phys.*, 7, 2585–2599, doi:10.5194/acp-7-2585-2007

Hatzianastassiou, N., Matsoukas, C., Fotiadi, A., Stackhouse Jr., P. W., Koepke, P., Pavlakis, K. G., and Vardavas, I., (2007b), “Modelling the direct effect of aerosols in the solar near-infrared on a planetary scale”, *Atmos. Chem. Phys.*, 7, 3211–3229, doi:10.5194/acp-7-3211-2007

Kinne, S., Lohmann, U., Feichter, J., Timmreck, C., Schulz, M., Ghan, S., Easter, R., Chin, M., Ginoux, P., Takemura, T., Tegen, I., Koch, D., Herzog, M., Penner, J., Pitari, G., Holben, B., Eck, T., Smirnov, A., Dubovik, O., Slutsker, I., Tanr´e, D., Torres, O., Mishchenko, M., Geogdzhayev, I., Chu, D. A., and Kaufman, Y. (2003), “Monthly



Averages of Aerosol Properties: A Global comparison among models, satellite data and AERONET ground data”, J. Geophys. Res, 108, 4634

Kistler, R., Kalnay, E., Collins, W., Saha, S., White, G., Woollen, J., Chelliah, M., Ebisuzaki, W., Kanamitsu, M., Kousky, V., van den Dool, H., Jenne, R., and Fiorino, M., (2001), ”The NCEP-NCAR 50 yr reanalysis: Monthly means CD-ROM and documentation, B. Am. Meteorol. Soc., 82, 247–267

Koepke, P., Hess, M., Schult, I., and Shettle, E. P., (1997), ”Global Aerosol Data Set. Report no 243”, Max-Planck Institut fuer Meteorologie, Hamburg, Germany, 44

Koo, B., Pandis, S. N., and Ansari, A., (2003), “Integrated approaches to modeling the organic and inorganic atmospheric aerosol components”, Atmos. Environ., 37, 4757–4768

Li, J., Wang, Z., Zhuang, G., Luo, G., Sun, Y., and Wang, Q. (2012). Mixing of Asian mineral dust with anthropogenic pollutants over East Asia: a model case study of a super-duststorm in March 2010, Atmos. Chem. Phys., 12, 7591-7607, doi:10.5194/acp-12-7591-2012

Malm W. C., Sisler J. F., Huffman D., Eldred R. A., Cahill T. A. (1994). Spatial and seasonal trends in particle concentration and optical extinction in the United States, J. Geophys. Res., 99(D1), pp. 1347–1370, doi: 10.1029/93JD02916

Malm W. C. (2000). Spatial and Seasonal Patterns and Temporal Variability of Haze and its Constituents in the United States: Report III, Chapter 3, US IMPROVE, pp. 3-5

Nenes, A., Pandis, S. N., and Pilinis, C., (1998), “ISORROPIA: a new thermodynamic equilibrium model for multiphase multicomponent inorganic aerosols”, Aquat. Geochem., 4, 123–152



Park, R. S., Song, C. H., Han, K. M., Park, M. E., Lee, S.-S., Kim, S.-B., and Shimizu, A. (2011). A study on the aerosol optical properties over East Asia using a combination of CMAQ-simulated aerosol optical properties and remote-sensing data via a data assimilation technique, *Atmos. Chem. Phys.*, 11, pp. 12275-12296, doi:10.5194/acp-11-12275-2011

Pilinis C. and Pandis S. N., (1995), “Physical, Chemical and Optical Properties of Atmospheric Aerosols”. *The handbook of Environmental Chemistry, Airborn Particulate Matter*, Springer, pp. 99 – 124.

Roy, B., Mathur, R., Gilliland, A. B. and Howard, S. C. (2007). A comparison of CMAQ-based aerosol properties with IMPROVE, MODIS, and AERONET data, *J. Geophys. Res.* 112, D14301

Rossow, W. B. and Schiffer, R. A., (1999), “Advances in understanding clouds from ISCCP”, *B. Am. Meteorol. Soc.*, 80, 2261–2287

Song, C. H., Park, M. E., Lee, K. H., Ahn, H. J., Lee, Y., Kim, J. Y., Han, K. M., Kim, J., Ghim, Y. S., and Kim, Y. J. (2008). An investigation into seasonal and regional aerosol characteristics in East Asia using model-predicted and remotely-sensed aerosol properties, *Atmos. Chem. Phys.*, 8, pp. 6627-6654, doi:10.5194/acp-8-6627-2008

Vardavas, I. and Carver, J. H., (1984),”Solar and terrestrial parameterizations for radiative convective models”, *Planet. Space Sci.*, 32, 1307–1325

Vardavas, I. M. and Taylor, F. W., (2011), “Radiation and Climate: Atmospheric energy budget from satellite remote sensing”, *International Series of Monographs on Physics No. 138*, Oxford University Press, Oxford

